On-Chip Hyperuniform Lasers for Controllable Transitions in Disordered Systems

Ronghui Lin, Valerio Mazzone, Nasir Alfaraj, Jianping Liu, Xiaohang Li,*
and Andrea Fratalocchi*

Designing light sources with controllable properties at the nanoscale is a main goal in research in photonics. Harnessing disorder opens many opportunities for reducing the footprints of laser devices, enabling physical phenomena and functionalities that are not observed in traditional structures. Controlling coherent light–matter interactions in systems based on randomness, however, is challenging especially if compared to traditional lasers. Here, how to overcome these issues by using semiconductor lasers created from stealthy hyperuniform structures is shown. An on-chip InGaN hyperuniform laser is designed and experimentally demonstrated, a new type of disordered laser with controllable transitions—ranging from lasing curve slopes, thresholds, and linewidths— from the nonlinear interplay between randomness and hidden order created via hyperuniformity. Theory and experiments show that the addition of degrees of order stabilizes the lasing dynamics via mode competition effects, arising between weak light localizations of the hyperuniform structure. The properties of the laser are independent from the cavity size or the gain material, and show very little statistical fluctuations between different random samples possessing the same randomness. These results open to on-chip lasers that combine the advantages of classical and random lasers into a single platform.

1. Introduction

Hyperuniformity[1,2] is a disordered phase of matter that enables a large variety of phenomena and applications including free form waveguides and resonators,[3–5] induced transparency,[6]

R. Lin, N. Alfaraj, Prof. X. Li
Department of Computer, Electrical and Mathematical Sciences and Engineering (CEMSE)
King Abdullah University of Science and Technology
Advanced Semiconductor Laboratory
Thuwal 23955-6900, Saudi Arabia
E-mail: xiaohang.li@kaust.edu.sa
Dr. V. Mazzone, Prof. A. Fratalocchi
Primalight
King Abdullah University of Science and Technology
Thuwal 23955-6900, Saudi Arabia
E-mail: andrea.fratalocchi@kaust.edu.sa
Prof. J. Liu
Suzhou Institute of Nano-Tech and Nano-Bionics
Chinese Academy of Sciences
Suzhou 215123, P. R. China

The ORCID identification number(s) for the author(s) of this article can be found under https://doi.org/10.1002/lpor.201800296

enhanced Raman spectroscopy,[7] and wavefront engineering via flat optics.[8,9] While the majority of current studies focus on linear properties of hyperuniform structures, effects arising from nonlinear effects are less known.

Many studies showed that coherent light amplification in disordered aggregates of nanostructures[10–20] enable functionalities that are not possible with traditional systems, ranging from speckle-free imaging,[21] to optofluidic sensing,[22] as well as low-threshold lasing in deep ultraviolet (UV) regions.[23,24] However, designing reproducible features with controllable properties in random structures is challenging, due to their unpredictable nature. The properties of disordered systems, in fact, change strongly from realization to realization and make it very difficult to control the system dynamic at large scales.[25] Even when 1D transitions between fully ordered and disordered systems are considered based on positional disorder,[12,26,27] the results show large fluctuation from sample to sample. The main problem is the number of parameters required to describe a random system, which is given by the position of all the scattering elements of the structure. This number grows linearly with the system size, generating manifolds of large dimensions that make it challenging to understand which direction to explore to achieve control over the system dynamics. This is different from classical lasers, in which the properties of the system are tuned by acting on few deterministic constraints.

Hyperuniform structures are potentially interesting in this field. Hyperuniform patterns are formed by physical processes that are governed by competing degrees of order and disorder.[28] If these dynamics are harnessed coherently in a single platform, it could open to a new class of disordered lasers in which the hidden degrees of order regulate the otherwise unpredictable dynamics of the random system.

In this article we address this problem by introducing on-chip hyperuniform lasers realized in $In_xGa_{1−x}N$ semiconductor, a widely used material for laser and light emitting diodes at visible wavelengths.[29,30] Our results show that this system supports controllable transitions from single mode to multimode lasing actions with different emission curves, threshold, and localization light patterns, opening up new applications of hyperuniform structures in laser engineering. The concept presented in this

ADVANCED
SCIENCE NEWS
www.advancedsciencenews.com

LASER
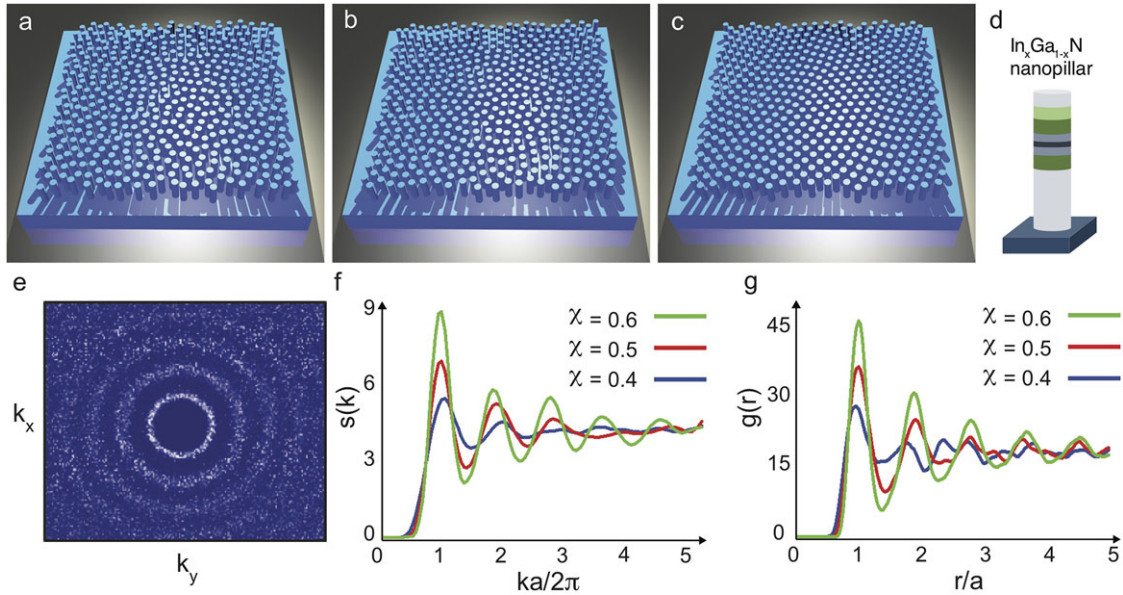& PHOTONICS
REVIEWS
www.lpr-journal.org

Figure 1. a–c) Semiconductor nanopillar arrays structures generated from different stealth hyperuniform patterns: $\chi = 0.4$ a), $\chi = 0.5$ b), and $\chi = 0.6$ c). d) Sketch of a single $In_xGa_{1-x}N$ nanopillar. e) Structure factor $S(\mathbf{k})$ in the reciprocal space for $\chi = 0.6$. f) Radial averaged structure factor $S(\mathbf{k})$ at different χ values. g) Radial distribution function for various χ values.

paper is very general and suitable to other direct bandgap materials, including InP, GaAs, and AlGaN semiconductors.

2. Design of Hyperuniform Lasers

Hyperuniform patterns are generated with the approach explained in refs. [31–34], which makes use of molecular dynamics simulations with particles subjected to the potential energy Φ.

$$\Phi = \sum_{|\mathbf{k}_m|<K} S(\mathbf{k}_m) = \frac{1}{N} \sum_{|\mathbf{k}_m|<K} \left| \sum_n e^{-i\mathbf{k}_m \mathbf{r}_n} \right|^2 \qquad (1)$$

where N is the total number of the particles, $\mathbf{r}_n$ their position, $\mathbf{k}_m$ a discrete wavenumber in the reciprocal space, and $S(\mathbf{k})$ the corresponding structure factor. Hyperuniform structure generated from Equation (1) is governed by the stealth parameter χ.

$$\chi = \frac{M(K)}{dN} \qquad (2)$$

with d the coordinate dimensions and $M(K)$ the number of wavevectors $\mathbf{k}_m$ supporting the stealthy condition $S(\mathbf{k}_m) = 0$ for $|\mathbf{k}| < K$.

The parameter χ regulates the hidden order in the hyperuniform lattice: the larger the χ, the deeper the minimum in the potential Φ, with the progressive formation of more ordered systems. **Figure 1**a–c shows this point quantitatively by illustrating hyperuniform structures generated for different χ in a square box of side $L = 5$ μm containing $N = 500$ particles, with each particle composed by an $In_xGa_{1-x}N$ nanopillar (Figure 1d) with diameter $d = 140$ nm. By increasing χ values we observe the generation of more ordered arrays structures, with traces of wavy crystalline patterns appearing at $\chi = 0.6$. Values above this limit

yield periodic crystals and are not here considered. Reducing the stealth parameter χ below $\chi = 0.4$ causes the bandgap to close, and as such it is not considered in this work. In all the considered range of values of χ, the structure is never periodic and always hyperuniform.

Figure 1e–g analyzes the structural properties of the hyperuniform patterns generated. Figure 1e shows the structure factor corresponding to the hyperuniform pattern of Figure 1c. The $S(\mathbf{k})$ shows the characteristic form that belongs to stealthy hyperuniform structures: a series of rings with isotropic response in all directions. Figure 1f presents the radially average structure factor at different χ, quantifying the progressive formation of a more ordered phase with peaks at specific Brillouin scattering directions. Figure 1g plots the corresponding radial distribution functions. Different hyperuniform patterns possess identical mean distance between the nanopillars, measured by the first peak in the $g(r)$.

Figure 2 provides an electromagnetic analysis of the hyperuniform structures by calculating photonic bandgap diagrams. The computations are carried with the MIT Photonic-Bands (MPB) package[35] over a super-cell composed of 500 particles, along the reciprocal lattice points $\Gamma = (0, 0)$, $X = (b/2, 0)$, $M = (b/2, b/2)$, where $b = 2\pi/L$ and L the length of the supercell side. Figure 2a–c plots the band diagrams for $\chi = 0.4$, 0.5, and 0.6, respectively. The bandgap between 360 and 417 nm falls within the emission range of $In_xGa_{1-x}N$ semiconductors.[36] Figure 2b,c,e,f illustrates that the width of the photonic bandgap is changed by the stealthy parameter χ, while the bandgap center position can be varied by acting on the diameter of the nanopillars. The difference arising from different realization of hyperuniform structures with same χ is small, especially at higher χ, illustrating good stability of this designing platform. The possibility to tune the bandgap in a disordered system with negligible variation between different sample possessing the same disorder is an effect of
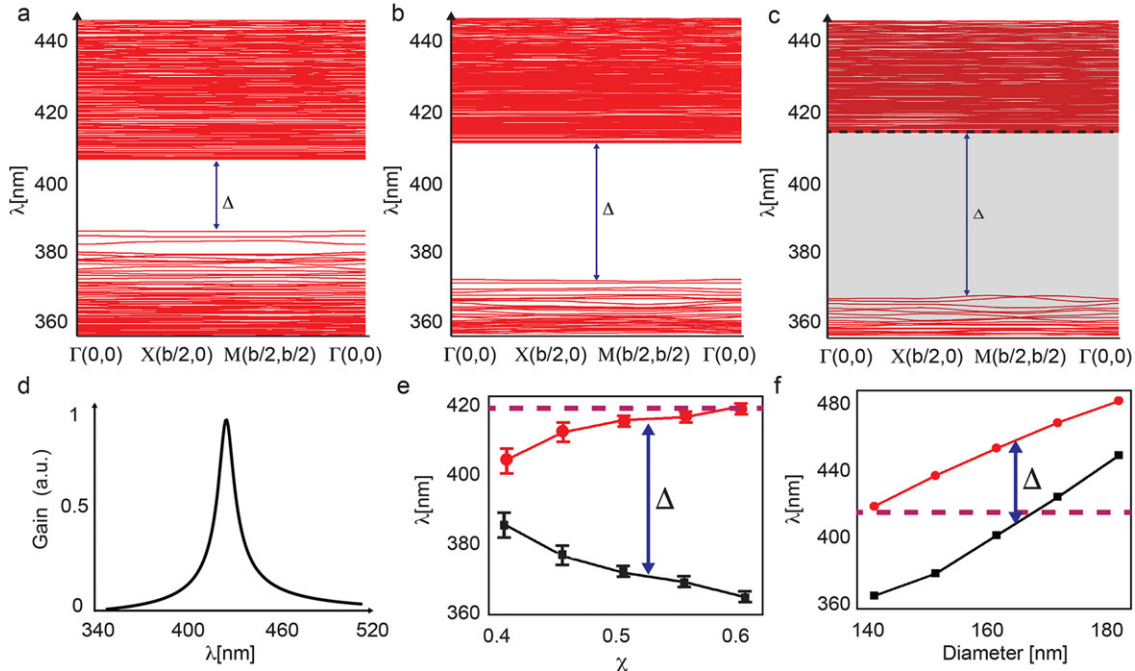
1800296 (2 of 9)

**ADVANCED
SCIENCE NEWS**

www.advancedsciencenews.com

LASER
&PHOTONICS
REVIEWS

www.lpr-journal.org

Figure 2. a–c) Band diagrams for $\chi = 0.4$, 0.5, and 0.6, respectively. The gray shaded area in c) indicates the variation of the emission range for $In_xGa_{1−x}N$ as a function of the In composition x; the dashed lines indicate the center wavelength emission of the nanopillar structure. d) Amplification bandwidth. e) Photonic bandgap as a function of the stealthy parameter χ and f) the nanopillar diameter.

hyperuniform correlations and enable a series of effects that we discuss in the next sections.

We designed our nanopillar array to emit near the band edge, where the density of electromagnetic states is higher.[31,37] To this extent, we consider $In_xGa_{1−x}N$ nanopillars with an emission centered at $\lambda = 416$ nm (Figure 2e, dashed line) and an amplification bandwidth of ≈ 20 nm[38] (Figure 2d), which is sufficiently large to overlap with the band edges of the hyperuniform arrays designed at different χ (Figure 2a–c).

3. Lasing Properties

3.1. Quantum Modeling

We use a rigorous Maxwell–Bloch approach for modeling the laser action of the hyperuniform structures. In this approach, Maxwell's equations are directly coupled with the quantum mechanical Bloch equations describing resonant light-induced transitions in atomic media.[39] Maxwell–Bloch equations provide a complete quantum mechanical treatment of light–matter interactions in gain media including gain saturation,[40] vectorial mode competitions,[39] and quantum noise.[41]

The quantum-mechanical formulation of the state of the atomic system is described by the set of energy eigenstates $|\phi_n\rangle$.

$$\mathbf{H}|\phi_n\rangle = \epsilon_n|\phi_n\rangle, \tag{3}$$

with $\mathbf{H}$ the total Hamiltonian operator and $|\phi_n\rangle$ the eigenstate with energy ϵ_n. If we consider a dipole-like interaction between

the electric field and the electrons of the material, the total Hamiltonian is decomposed by a displacement part, defined by a displacement operator $\hat{Q}$, and an unperturbed term $\mathbf{H}_0$.

$$\hat{\mathbf{H}} = \hat{\mathbf{H}}_0 + e\mathbf{E}\hat{Q} \tag{4}$$

The Hamiltonian Equation (4) generates a nonlinear polarization term $\mathbf{P}_{NL}$ in Maxwell's equations, depending on the expectation value of the displacement operator $\hat{\mathbf{Q}}$.

$$\mathbf{P}_{NL} = -e\rho_0 < \hat{Q} > (t) \tag{5}$$

where e is the electric charge, ρ_0 is the carrier density (proportional to the pumping rate), and $< \hat{Q} >$ is the quantum expectation of the operator with respect to the time-dependent state of the system.

The nonlinear polarization term is then added to the dispersive linear material polarization $P_{lin} = \epsilon_0 \int dt' \eta(t − t')\mathbf{E}(t')$, with η the noninstantaneous linear susceptibility, to account for the complete polarization response of the active system $P = P_{lin} + P_{Nlin}$. The full set of equations are as follows:

$$\begin{cases} \partial_t\mathbf{H} = -\frac{1}{\mu_0}\nabla \times \mathbf{E} \\ \partial_t\mathbf{E} = \frac{1}{\epsilon_0}[\nabla \times \mathbf{H} - \partial_t(\mathbf{P}_{lin} + \mathbf{P}_{Nlin})] \\ \mathbf{P}_{lin}(t) = \epsilon_0 \int dt' \eta(t − t')\mathbf{E}(t') \\ \mathbf{P}_{Nlin} = eq_0\rho_0[S_1\hat{\mathbf{x}} + S_4\hat{\mathbf{y}} + S_9\hat{\mathbf{z}}] \\ \partial_t S_l = \sum \Gamma_{lm}S_m - \frac{1}{\tau_l}[S_l - S_l^{(0)}] \end{cases} \tag{6}$$
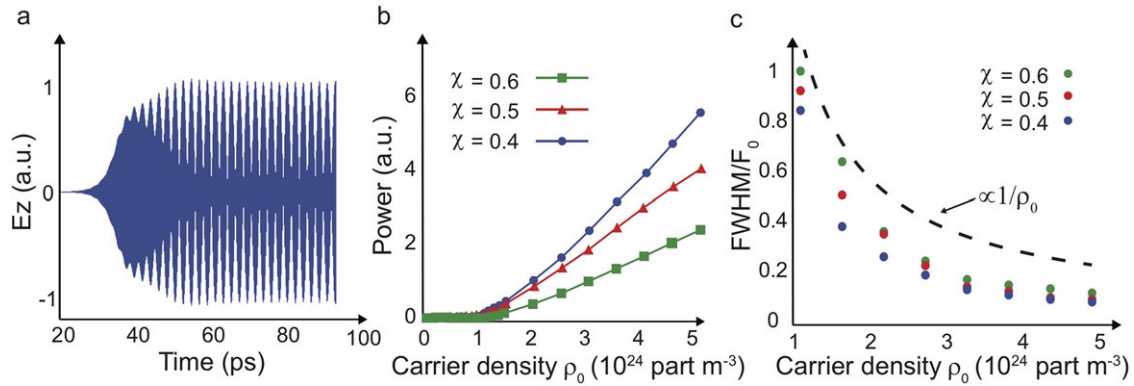
**ADVANCED
SCIENCE NEWS**
www.advancedsciencenews.com

LASER
& PHOTONICS
REVIEWS

www.lpr-journal.org

Figure 3. a) Time evolution of the electric field amplitude E_z for $\chi = 0.6$ and carrier density $\rho_0 = 2 \times 10^{24}$ part m^{-3}. b) Lasing input–output curves as a function of carrier density ρ_0 and hyperuniform stealthy parameter χ. c) Lasing full width half maximum (FWHM) normalized respect to the value at threshold FWHM$_0$, as a function of carrier density ρ_0.

The first two equations are Maxwell's equations describing the evolution of electric field **E** and magnetic field **H**, with μ_0 and ϵ_0 are the vacuum permeability and permittivity, respectively. The second and the third equations describe the linear and nonlinear contribution of the atomic polarization, with q_0 the atomic length scale. The last equation describes the evolution of the density matrix as a function of the coherence vector **S**, whose components are defined as $S_j = Tr(\hat{\rho}\lambda_j)$, with Tr the trace operator, Γ_{lm} the coupling coefficients (expressions are found in ref. [39]) and τ_l atomic decay constants, which is chosen as 0.9 ns and 100 fs, respectively for carrier lifetime and carrier dephasing time according to the literature for In$_x$Ga$_{1-x}$N semiconductors.[42] The refractive index is chosen to be 2.5, which corresponds to the average index of In$_x$Ga$_{1-x}$N materials. As the samples are composed by 2D patterns of in-plane lasing nanopillars, we theoretically studied the lasing properties of the system by a campaign of 2D simulations. The resolution used in our simulation was 5 nm and the computational box were 6 μm by 6 μm for each lasing structure. At each value of χ, we generated a statistical populations of 20 samples, and analyzed them in a parallel simulation campaign of the duration of 1 month time.

3.2. Input–Output Curve and Emission Linewidth

Figure 3 shows lasing curves corresponding to the different hyperuniform systems of Figure 1. Figure 3a plots the electric field E_z evolution for $\chi = 0.6$ and probed in a point outside the nanopillars. The lasing action started at around $t = 35$ ps, and reached a steady state after 60 ps. Figure 3b shows lasing input–output curves as a function of the carrier density ρ_0 for different hyperuniform patterns, and Figure 3c plots the full width half maximum (FWHM) of the lasing spectra. The output power is calculated by integrating over all the emission wavelengths. The curves show the typical behavior of semiconductor lasers, with a linear output power increase after a lasing threshold, and an equivalent Schawlow–Townes law with $FWHM \propto \frac{1}{\rho_0}$ for the lasing spectra.

The lasing threshold ρ_c of these structures changed with the stealthiness of the structure, increasing from $\rho_c = 1.2 \times 10^{24}$ part · m^{-3} ($\chi = 0.4$) to $\rho_c = 2 \times 10^{24}$ part · m^{-3} ($\chi = 0.6$).

These results showed that a hyperuniform structure with less order is more advantageous in terms of laser power and threshold with respect to a more ordered configuration, even if the latter showed a wider photonic bandgap (Figure 2b).

Figure 3b shows that the slope of the input–output lasing curve in the hyperuniform laser array can be changed by varying the stealthy parameter χ, with $\chi = 0.4$ being the highest. The laser output power for $\chi = 0.4$ was 2.3 times that of $\chi = 0.6$ at $\rho_0 = 5 \times 10^{24}$ part · m^{-3} carrier density.

In a classical laser, controlling the emission power is achieved by a suitable design of the quality factor of the laser cavity modes. This requires changing the characteristic dimension of the cavity for adjusting the mode spectral linewidth. In random lasers, conversely, predicting the quality factor of the modes is a more difficult task, due to the strong fluctuations observed in different sample realizations with the same statistical disorder.

Despite their random nature, lasers designed with hyperuniform structures enables the possibility to change the lasing curve with minimal fluctuations and by using a single degree of freedom regulating their stealthiness. As an advantage compared to classical cavities, hyperuniform lasers offer the possibility to adjust the laser emission without altering the size of the structure. This originates from the fact that in these random structures cavity modes are generated from scattering effects. This allows to change their localized nature from the scattering pattern generated, without altering the system size. This point is quantitatively discussed in the next section.

3.3. Modes Competition Effects

Figure 4 analyzes nonlinear mode competition effects by calculating lasing spectra at fixed carrier density $\rho_0 = 2 \times 10^{24}$ part · m^{-3} and different χ (Figure 4a), with corresponding spectrograms (Figure 4b) and spatial electromagnetic energy distribution of the modes (Figure 4c).

The lowest lasing wavelengths is located at $\lambda = 405$ nm ($\chi = 0.4$), $\lambda = 412$ nm ($\chi = 0.5$), and $\lambda = 416$ nm ($\chi = 0.6$), and corresponds to the wavelength position of the upper band edge of the structure (Figure 2b). Remaining lasing wavelengths are located within 10 nm from the band edge. The power density
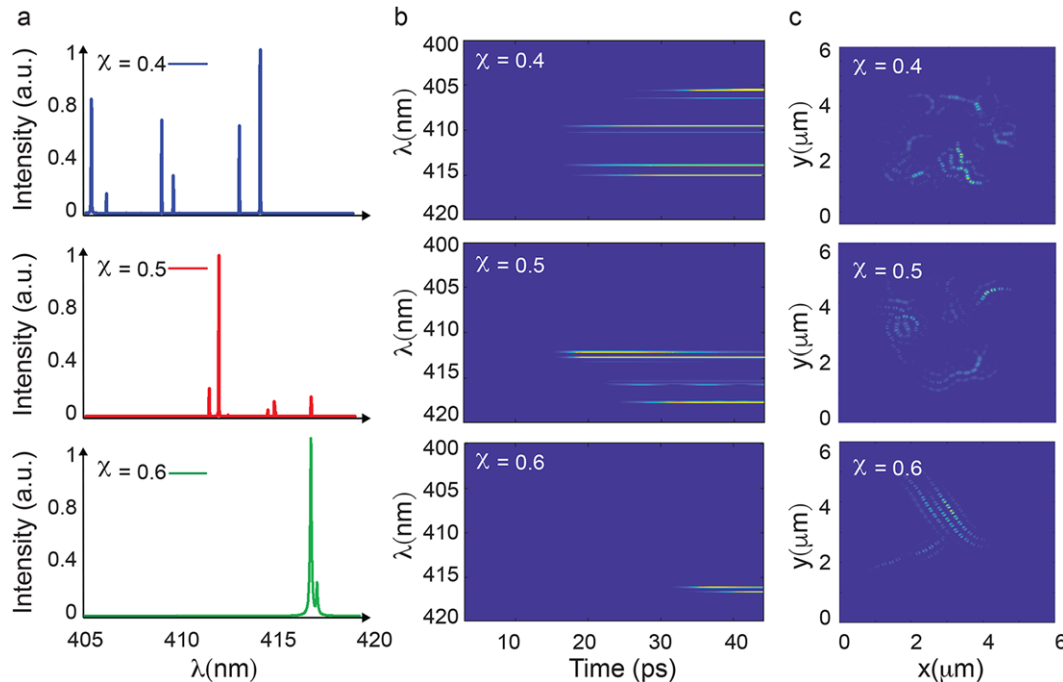
Figure 4. a) Lasing power density spectra for different hyperuniform structures at constant carrier density $\rho_0 = 2 \times 10^{24}$ part · m^{-3} for different stealthiness χ. b) Corresponding spectrograms and c) section along the (x, y) plane of the electromagnetic energy distribution of the lasing modes.

spectra show that in a hyperuniform structure the number of lasing modes is changed by varying the stealthy parameter χ. The hyperuniform laser is highly multimodal at $\chi = 0.4$ (more disordered) and progressively becomes almost monomodal at $\chi = 0.6$ (more ordered).

This behavior originates from the bandgap tuning in the hyperuniform lattice, which increases the number of localized modes with higher quality factors at stronger disorder χ, thus favoring their lasing emission at lower lasing thresholds. Figure S1, Supporting Information, shows the calculated modes of the linear hyperuniform structure for different values of χ. The modes are all localized, similar to previous reports,[4] and present different localization degrees for different stealthiness χ. This depends on the fact that changing χ implies the introduction of different degrees of order in the disordered hyperuniform pattern, thus modifying the localization strength of the modes. We calculated the quality factor Q_n of the lasing modes shown in Figure 4 by first decomposing the lasing spectrum into eigenmodes of the hyperuniform system and by then calculating the corresponding lifetime from the power density spectrum. At $\chi = 0.4$, we found six lasing modes with $Q_1 = 23531$, $Q_2 = 25429$, $Q_3 = 35632$, $Q_4 = 34425$, $Q_5 = 35328$, $Q_6 = 34172$ ($\bar{Q} = 31419 \pm 4962$). At $\chi = 0.5$, we found four lasing modes with $Q_1 = 35243$, $Q_2 = 34524$, $Q_3 = 26437$, $Q_4 = 25932$ ($\bar{Q} = 30534 \pm 4360$). At $\chi = 0.6$, we found a single lasing mode with $Q = 20484$.

This analysis shows a clear a trend in reducing the number of competing modes and their Q factor for increasing χ, that is, for increasing order in the structure. By injecting order in the structure the lasing action passes from a multi-mode regime at $\chi = 0.4$, with highly localized and high Q modes, to single mode lasing at $\chi = 0.6$, with a single mode possessing a more extended spatial profile. By changing the stealth parameter χ, it is therefore

possible to adjust the number of modes excited and their spatio-temporal localizations, providing a transition from multi-mode to single mode lasing.

This result is also illustrated in detail in Figure4b: the time-dependent spectrogram for $\chi = 0.4$, $\chi = 0.5$ and $\chi = 0.6$ clearly shows the competition of highly localized modes with progressive higher quality factors, proved by their earlier excitation in the lasing dynamics at increasing χ. Hosting more localized modes with higher quality factors induces a higher energy emission for the same pumping rate, which explains the physical origin of the phenomenon observed in Figure 3b. This results originate from the fact that high Q modes have longer lifetimes and trap electromagnetic energy efficiently; when actively pumped, these modes reach lasing stage at lower pumping thresholds.[43]

The mode interactions cause the spectrum to fluctuate on a time scale of tens of picoseconds, which is consistent with experimental data obtained by steak camera.[44] This trend is also confirmed by simulating structures of larger size. Figures S2 and S3, Supporting Information, show lasing spectra and spectrograms for larger structures (four times bigger) with different χ values.

These results represent a crossing point between ordered and disordered materials. In a classical laser, changing the number of modes is possible at the expense of the size of the laser, for example by modifying the cavity length, or by changing the amplification bandwidth of the gain material. In random lasers, the emission typically changes from one to a large number of modes following a condensation process equivalent to a Schawlow–Townes law.[13] In a hyperuniform structure, conversely, we can adjust all the modal properties of the system without changing the size of the structure and by acting only on the stealthy parameter χ, that is, by increasing or decreasing the order degree of the structure.
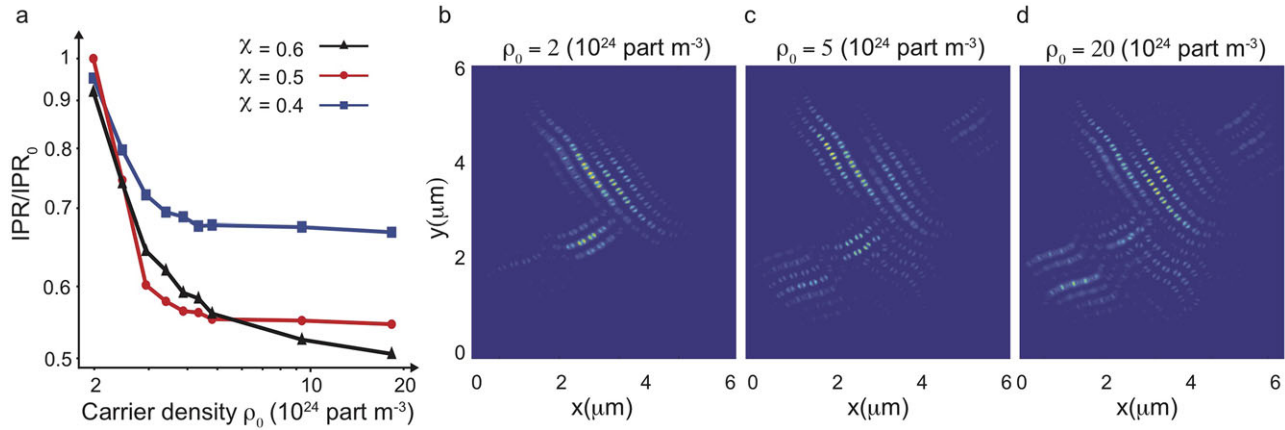
Figure 5. a) IPR as a function of carrier density ρ_0 for various χ normalized to the initial value IPR_0. b–d) Section along the (x, y) plane of the spatial distribution of the electromagnetic energy for $\chi = 0.6$ at various carrier densities ρ_0.

3.4. Nonlinear Light Localization

A phenomenon that appears in random structures but is absent in ordered systems is the existence of localized modes.[45] It has been recently shown that linear hyperuniform structures support light localization dynamics with different characteristic lengths.[46] We here investigate the effects arising from the presence of nonlinearity induced by the lasing action. To characterize the degree of energy localization in the excited lasing modes, we used the standard inverse participation ratio (IPR).[47]

$$IPR = \frac{\int_{V_{tot}} |E(\mathbf{r})|^4 d\mathbf{r}}{\left(\int_{V_{tot}} |E(\mathbf{r})|^2 d\mathbf{r}\right)^2} \cdot V_{tot} \qquad (7)$$

where V_{tot} is the total volume and $E(\mathbf{r})$ is the electric field amplitude. **Figure 5**a plots the resulting IPR for different carrier density and χ. This analysis shows that in a hyperuniform structure the characteristic localization length of the modes changes nonlinearly, with variations up to 50%. In a hyperuniform structure, the IPR sharply decreases with the increasing of the carrier density ρ_0, and reaches a plateau at high carrier densities. This behavior seems universal, that is, it does not depends on the specific hyperuniform pattern considered.

To understand the origin of this effect, we calculate in Figure 5b–d the spatial distribution of the mode patterns corresponding to one structure ($\chi = 0.6$) with increasing carrier densities $\rho_0 = 2 \times 10^{24}$ part m^{-3} b), $\rho_0 = 5 \times 10^{24}$ part m^{-3} c), and $\rho_0 = 20 \times 10^{24}$ part m^{-3} d). This analysis show that larger carrier densities induce a larger number of localized modes, which are spatially localized in different regions of the hyperuniform structure. This process decreases the overall localization length of light energy and reduces the IPR.

Contrary to intuition, nonlinear induced localization is stronger in a more ordered hyperuniform structure, indicating that in this system the excitation of nonlinear modes at higher intensities originate localized energy spots at a reduced distance between each others.

4. Experimental Results: On-Chip Nanofabrication and Lasing Characterization

We realized on-chip hyperuniform lasers with different stealth parameters χ by using a top-down etching method on an edge emitting blue laser heterostructure[48] composed of an $n - GaN$ buffer layer, a $In_xGa_{1-x}N/GaN$ multiple quantum well (MQW) active region ($x = 10\%$) sandwiched between two $In_xGa_{1-x}N$ waveguiding layers ($x = 5\%$) and two $Al_xGa_{1-x}N$ cladding layers ($x = 8\%$). The laser structure also includes an $Al_xGa_{1-x}N$ electron block layer (EBL) with $x = 20\%$ (**Figure 6**a). The MQW region has the highest refractive index, guiding emitted light in the xy plane (Figure 6a, index profile). The structure can be pumped both optically and electrically via, for example, a 2D conductive material as a top electrode. In this work, we illustrate results obtained via optical pumping.

To fabricate the nanopillars with the desired hyperuniform pattern, the wafer is first rinsed with acetone, IPA, and water. Subsequently a photoresist (PMMA) layer of 200 nm is spin-coated on top of the wafer and exposed by electron beam lithography, followed by a Ni hard metal mask of thickness 75 nm via electron beam evaporation. After the lift-off, the sample undergoes a dry-etching process in which the nanopillars arranged in the desired hyperuniform pattern are created.

The fabricated structures, characterized at the scanning electron microscope (SEM), showed hyperuniform pillar patterns with an average inter-pillar distance $a = 350$ nm, pillar radius $r = 90$ nm, and height 1.2 µm. Figure 6b–d shows SEM images of large scale fabricated samples for different values of the parameter $\chi = 0.4$, 0.5 and 0.6, respectively, in which the total area covered by each of the hyperuniform structure is 2 mm × 2 mm, which is larger than the one reported by on-chip lasers emitting in the visible realized with periodic and random systems.[49–54] The insets in Figure 6b–d illustrates zoomed magnifications of the fabricated pillars with experimentally calculated radial distribution functions (RDFs).

We characterized stimulated emission spectra by using the the optical pumping setup illustrated in Figure 6e. An KrF (kripton fluoride) excimer laser emitting at 248 nm and operating at 1 Hz repetition rate is used as pumping source. The laser emission is
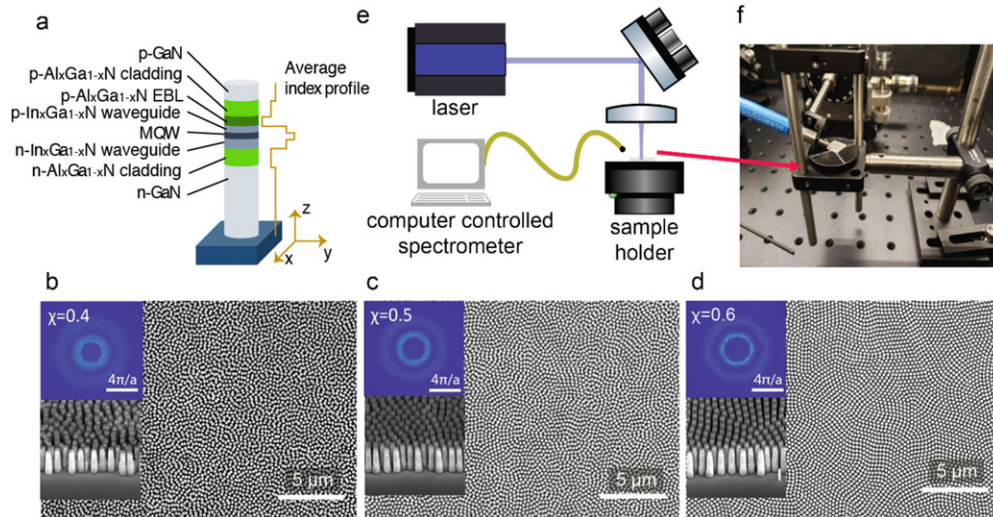
ADVANCED
SCIENCE NEWS
www.advancedsciencenews.com

LASER
& PHOTONICS
REVIEWS

www.lpr-journal.org

Figure 6. a) Material composition of the single nanopillar. b–d) Scanning electron microscope images of the realized sample for χ = 0.4, 0.5, and 0.6. The insets show tilted SEM images of the nanopillars arranged in the hyperuniform pattern with respective radial distribution functions. e) Sketch of the experimental setup. f) Photo of a fabricated sample on its holder during measurements.
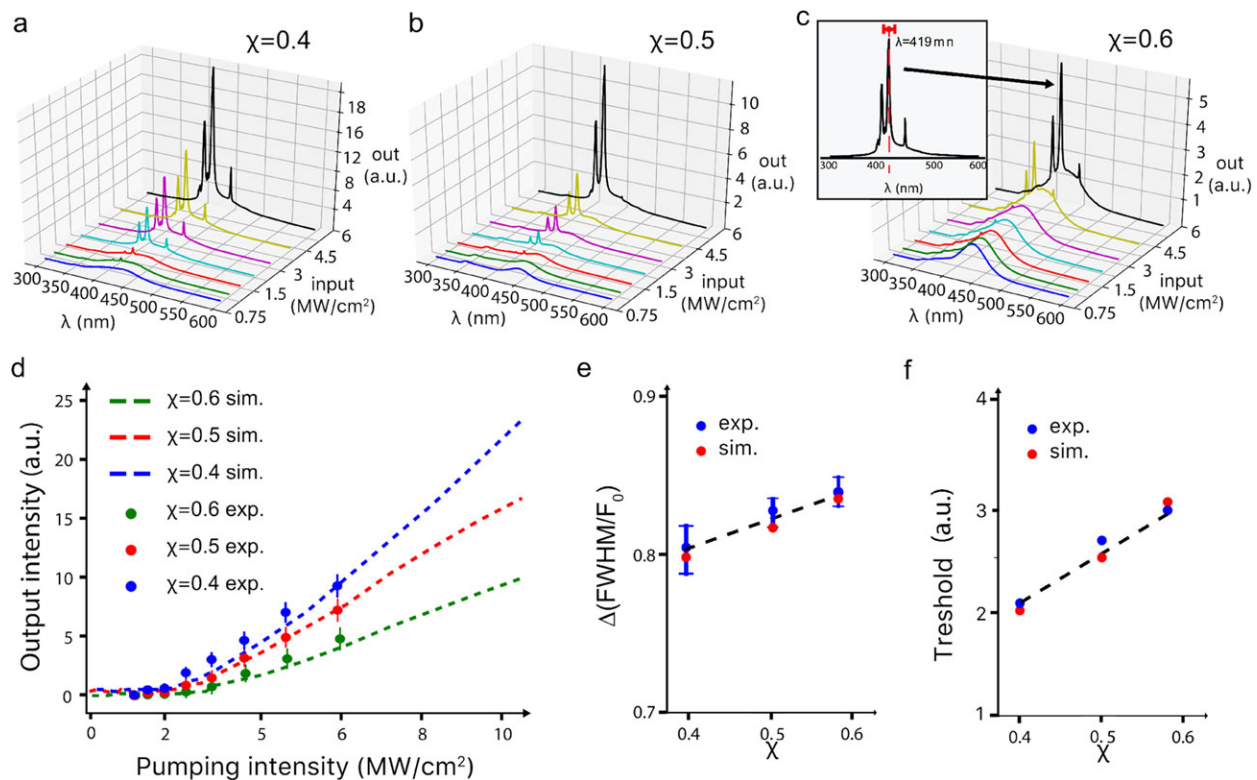

Figure 7. a–c) Emission spectra for χ = 0.4, 0.5, and 0.6, respectively. d) Comparison between simulations and experiments for the intensity input/output curves at χ = 0.4 (blue), χ = 0.5 (red), and χ = 0.6 (green). e) Comparison between experiments and simulations of lasing linewidths and f) lasing thresholds as a function of the parameter χ.

focused on the sample by a plano convex lens with focal length f = 40 mm. The emission from the hyperuniform sample is then collected by a fiber optical spectrum analyzer with 0.7 nm resolution. Figure 6f shows a detail of optical fiber collecting the signal from the device mounted on the sample holder.

Figure 7a–c displays power density spectra of samples characterized by different values of the parameter χ, before and after lasing threshold. The inset in Figure 7c shows a zoomed detail of the spectrum at the pumping intensity 6 MW cm^{-2}. The main emission peak at 419 nm correspond to the emission bandwidth of the
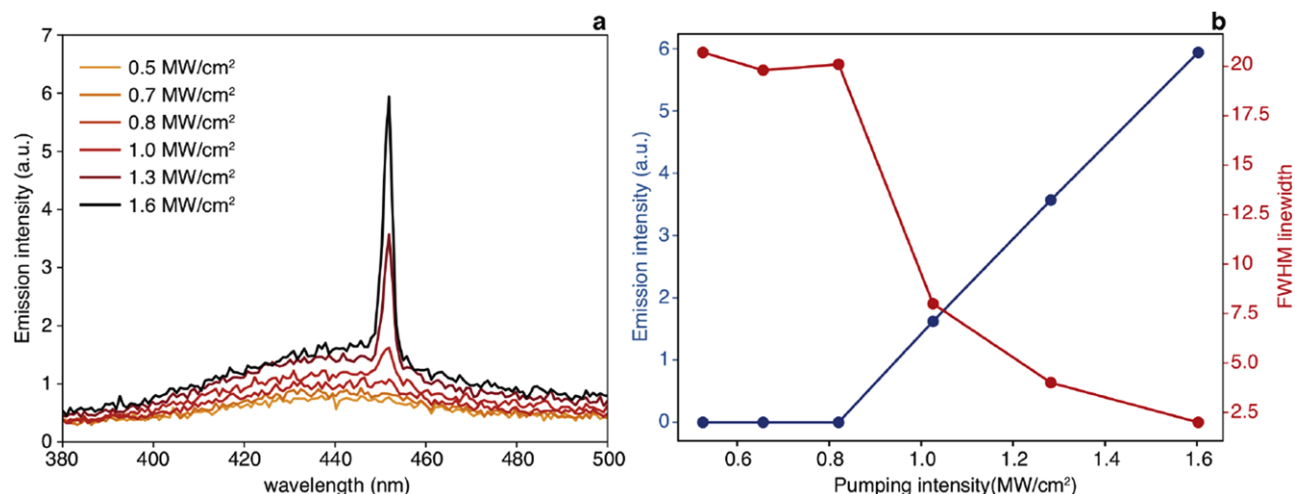
Figure 8. Comparative experiments on planar samples: a) emission spectra with b) input–output curves (blue lines) and FWHM linewidths (red line) for increasing optical pumping rates.

MQW and perfectly agrees to the predicted emission values of these structures (Figure 7c, red bar), as shown in Figure 2e. The two sideband emission peaks correspond to the emission of GaN waveguiding and cladding layers due to effective confinement of light in the vertical directions in these layers. The stimulated emission threshold of the structure lines between 1-2 MW cm^{-2}, well within the range of experimental values of available literature in GaN/InGaN nanowires[49–52] and ZnO nanorods.[53,54]

Figure 7d–f provides a detailed comparison between theoretical predictions and experimental results. Figure 7d compares input/output emission curves of hyperuniform samples fabricated at different stealth parameter χ (markers) with theoretical estimates (dashed lines). The FDTD analysis provides results in excellent agreement with experiments, showing the tuning of emission curves both in emission intensity and stimulated emission threshold. The experiments confirmed that hyperuniform structures provide stable and reproducible effects with low standard deviations between different hyperuniform samples possessing the same stealthiness, especially at higher χ.

In Figure 7e,f, finally, we plot the FWHM linewidth and the stimulated emission threshold acquired from experiments (markers) and predicted by theory (dashed line) for different values of χ. The experiments confirmed that the threshold is changed by increasing the value of the stealth parameter χ. Figure S4, Supporting Information, shows the full behavior of the emission linewidth for varying pumping rates and χ factors. In complete agreement with published data on planar In$_x$Ga$_{1-x}$N/GaN electrically pumped lasers,[48] the occurrence of stimulated emission reduces the linewidths down to values between 2 and 3 nm.

To provide a further comparison on the emission spectra from hyperuniform samples, we performed additional experiments on planar structures with no hyperuniform pattern. **Figure 8** summarizes the results. The samples show linewidth reductions up to 2.5 nm, in agreement with the results of hyperuniform samples, and a stimulated emission threshold of 0.8-1 MW cm^{-2}, which is slightly below the results obtained with hyperuniform structures. This depends on the fact that the realization of a hyperuni-

form pattern of nanodisks on a planar sample, even if achieved with good vertical accuracy as shown in Figure 6, inevitably introduces surface defect states that increase carrier recombination rate, leading to a slightly higher threshold for the occurrence of stimulated emission.

5. Conclusions

We proposed a new type of on-chip disordered laser in which competing degrees of order are used to govern its dynamics. The system is composed of hyperuniform nanopillar arrays realized on an edge emitting In$_x$Ga$_{1-x}$N semiconductor. We showed that localized band edge modes support spatio-temporal lasing dynamics that are changed from a single parameter, which regulates the stealthiness of the structure and the nonlinear interplay between order and disorder in the laser array. Hyperuniform structures with more disorder facilitate laser emission with lower threshold and higher output power. Lasing occurs within ≈10 nm from the band edge with the possibility to tune the lasing input–output curves, thresholds, and laser linewidths, with minimal statistical deviations from different disordered realizations possessing the same stealthiness χ. An advantage of hyperuniform lasers is to access the properties of disordered systems within a design platform that is very stable against fabrication tolerances, as experimentally proved by the good agreement between theory and experiments on samples fabricated on large dimensions of a few millimeters. The idea explored in this work can be generalized to different types of semiconductors and can open new types of integrated, on-chip, optoelectronic applications of disordered lasers.

Supporting Information

Acknowledgements

Conflict of Interest

The authors declare no conflict of interest.

Keywords

[1] S. Torquato, *Phys. Rep.* **2018**, *745*, 1.

[2] J. Kim, S. Torquato, *Phys. Rev. B* **2018**, *97*, 054105.

[3] W. N. Man, M. Florescu, E. P. Williamson, Y. Q. He, S. R. Hashemizad, B. Y. C. Leung, D. R. Liner, S. Torquato, P. M. Chaikin, P. J. Steinhardt, *Proc. Natl. Acad. Sci. USA* **2013**, *110*, 15886.

[4] T. Amoah, M. Florescu, *Phys. Rev. B* **2015**, *91*, 020201.

[5] M. Florescu, P. J. Steinhardt, S. Torquato, *Phys. Rev. B* **2013**, *87*, 165116.

[6] O. Leseur, R. Pierrat, R. Carminati, *Optica* **2016**, *3*, 763.

[7] C. De Rosa, F. Auriemma, C. Diletto, R. Di Girolamo, A. Malafronte, P. Morvillo, G. Zito, G. Rusciano, G. Pesce, A. Sasso, *Phys. Chem. Chem. Phys.* **2015**, *17*, 8061.

[8] M. Castro-Lopez, M. Gaio, S. Sellers, G. Gkantzounis, M. Florescu, R. Sapienza, *APL Photonics* **2017**, *2*, 061302.

[9] N. Muller, J. Haberko, C. Marichy, F. Scheffold, *Optica* **2017**, *4*, 361.

[10] R. Weill, B. Fischer, O. Gat, *Phys. Rev. Lett.* **2010**, *104*, 173901.

[11] D. S. Wiersma, *Nat. Phys.* **2008**, *4*, 359.

[12] C. Conti, A. Fratalocchi, *Nat. Phys.* **2008**, *4*, 794.

[13] C. Conti, M. Leonetti, A. Fratalocchi, L. Angelani, G. Ruocco, *Phys. Rev. Lett.* **2008**, *101*, 143901.

[14] M. Leonetti, C. Conti, C. Lopez, *Nat. Photon.* **2011**, *5*, 615.

[15] S. Schönhuber, M. Brandstetter, T. Hisch, C. Deutsch, M. Krall, H. Detz, A. M. Andrews, G. Strasser, S. Rotter, K. Unterrainer, *Optica* **2016**, *3*, 1035.

[16] T. Hisch, M. Liertzer, D. Pogany, F. Mintert, S. Rotter, *Phys. Rev. Lett.* **2013**, *111*, 023902.

[17] H. K. Liang, B. Meng, G. Liang, J. Tao, Y. Chong, Q. J. Wang, Y. Zhang, *Adv. Mater.* **2013**, *25*, 6859.

[18] M. Lee, S. Callard, C. Seassal, H. Jeon, *Nat. Photon.* **2019**, *13*, 445.

[19] M. Tonouchi, *Nat. Photonics* **2007**, *1*, 97.

[20] N. Ghofraniha, I. Viola, F. Di Maria, G. Barbarella, G. Gigli, L. Leuzzi, C. Conti, *Nat. Commun.* **2015**, *6*, 6058.

[21] B. Redding, M. A. Choma, H. Cao, *Nat. Photon.* **2012**, *6*, 355.

[22] X. D. Fan, S. H. Yun, *Nat. Methods* **2014**, *11*, 141.

[23] K. H. Li, X. Liu, Q. Wang, S. Zhao, Z. Mi, *Nat. Nanotechnol.* **2015**, *10*, 140.

[24] M. Suja, S. B. Bashar, B. Debnath, L. X. Su, W. H. Shi, R. Lake, J. L. Liu, *Sci. Rep.* **2017**, *7*, 2677.

[25] J. Liu, P. D. Garcia, S. Ek, N. Gregersen, T. Suhr, M. Schubert, J. Mørk, S. Stobbe, P. Lodahl, *Nat. Nanotechnol.* **2014**, *9*, 285.

[26] G. Fujii, T. Matsumoto, T. Takahashi, T. Ueta, *Opt. Express* **2012**, *20*, 7300.

[27] K. C. Kwan, X. M. Tao, G. D. Peng, *Opt. Lett.* **2007**, *32*, 2720.

[28] Y. Jiao, T. Lau, H. Hatzikirou, M. Meyer-Hermann, J. C. Corbo, S. Torquato, *Phys. Rev. E* **2014**, *89*, 022721.

[29] R. H. Lin, S. V. Galan, H. D. Sun, Y. R. Hu, M. S. Alias, B. Janjua, T. K. Ng, B. S. Ooi, X. H. Li, *Photon. Res.* **2018**, *6*, 457.

[30] J. B. Wright, S. Liu, G. T. Wang, Q. M. Li, A. Benz, D. D. Koleske, P. Lu, H. W. Xu, L. Lester, T. S. Luk, I. Brener, G. Subramania, *Sci. Rep.* **2013**, *3*, 2982.

[31] L. S. Froufe-Perez, M. Engel, P. F. Damasceno, N. Muller, J. Haberko, S. C. Glotzer, F. Scheffold, *Phys. Rev. Lett.* **2016**, *117*, 053902.

[32] R. D. Batten, F. H. Stillinger, S. Torquato, *J. Appl. Phys.* **2008**, *104*, 033504.

[33] S. Torquato, G. Zhang, F. H. Stillinger, *Phys. Rev. X* **2015**, *5*, 021020.

[34] O. U. Uche, F. H. Stillinger, S. Torquato, *Phys. Rev. E* **2004**, *70*, 046122.

[35] S. G. Johnson, J. D. Joannopoulos, *Opt. Express* **2001**, *8*, 173.

[36] S. Nakamura, *Semicond. Sci. Technol.* **1999**, *14*, R27.

[37] L. S. Froufe-Pérez, M. Engel, J. J. Sáenz, F. Scheffold, *Proc. Natl. Acad. Sci. USA.* **2017**, *114*, 9570.

[38] G. Orsal, Y. E. Gmili, N. Fressengeas, J. Streque, R. Djerboub, T. Moudakir, S. Sundaram, A. Ougazzaden, J. Salvestrini, *Opt. Mater. Express* **2014**, *4*, 1030.

[39] A. Fratalocchi, C. Conti, G. Ruocco, *Phys. Rev. A* **2008**, *78*, 013806.

[40] H. F. Hofmann, O. Hess, *Phys. Rev. A* **1999**, *59*, 2342.

[41] J. S. Totero Gongora, A. E. Miroshnichenko, Y. S. Kivshar, A. Fratalocchi, *Laser Photon. Rev.* **2016**, *10*, 432.

[42] D. L. Boiko, P. P. Vasil'ev, *Opt. Express* **2012**, *20*, 9501.

[43] H. Haus, *Waves and Fields in Optoelectronics*, Prentice Hall, Upper Saddle River, NJ **1984**.

[44] S. García-Revilla, J. Fernández, M. Barredo-Zuriarrain, L. D. Carlos, E. Pecoraro, I. Iparraguirre, J. Azkargorta, R. Balda, *Opt. Express* **2015**, *23*, 1456.

[45] F. Haake, *Quantum Signatures of Chaos*, 3rd ed., Springer, Berlin **2010**.

[46] G. M. Conley, M. Burresi, F. Pratesi, K. Vynck, D. S. Wiersma, *Phys. Rev. Lett.* **2014**, *112*, 143901.

[47] S. Imagawa, K. Edagawa, K. Morita, T. Niino, Y. Kagawa, M. Notomi, *Phys. Rev. B* **2010**, *82*, 115116.

[48] J. Liu, L. Zhang, D. Li, K. Zhou, Y. Cheng, W. Zhou, A. Tian, M. Ikeda, S. Zhang, H. Yang, *IEEE Photon. Technol. Lett.* **2017**, *29*, 2203.

[49] M. Behzadirad, M. Nami, N. Wostbrock, M. R. Zamani Kouhpanji, D. F. Feezell, S. R. J. Brueck, T. Busani, *ACS Nano* **2018**, *12*, 2373.

[50] M. Sakai, Y. Inose, K. Ema, T. Ohtsuki, H. Sekiguchi, A. Kikuchi, K. Kishino, *Appl. Phys. Lett.* **2010**, *97*, 151109.

[51] J. B. Wright, S. Liu, G. T. Wang, Q. Li, A. Benz, D. D. Koleske, P. Lu, H. Xu, L. Lester, T. S. Luk, I. Brener, G. Subramania, *Sci. Rep.* **2013**, *3*, 2982.

[52] A. Hurtado, H. Xu, J. B. Wright, S. Liu, Q. Li, G. T. Wang, T. S. Luk, J. J. Figiel, K. Cross, G. Balakrishnan, L. F. Lester, I. Brener, *Appl. Phys. Lett.* **2013**, *103*, 251107.

[53] H. Y. Yang, S. P. Lau, S. F. Yu, A. P. Abiyasa, M. Tanemura, T. Okita, H. Hatano, *Appl. Phys. Lett.* **2006**, *89*, 011103.

[54] R. Niyuki, H. Fujiwara, Y. Ishikawa, N. Koshizaki, T. Tsuji, K. Sasaki, *J. Opt.* **2016**, *18*, 035202.